Arch. Min. Sci. **70** (2025), 4, 575-596

Electronic version (in color) of this paper is available: http://mining.archives.pl

DOI: https://doi.org/10.24425/ams.2025.157448

ANNA PAJDAK[1*], ADAM DĘBSKI[2], MATEUSZ KUDASIK[1], NORBERT SKOCZYLAS[3], WOJCIECH MAZIARZ[2], WŁADYSŁAW GĄSIOR[2]

THERMAL EFFECTS ACCOMPANYING HYDROGEN ACCUMULATION IN CARBON AND COAL STRUCTURES

The article presents a comprehensive analysis of hydrogen accumulation properties on various carbon and coal structures, including carbon nanotubes of different diameters, reduced graphene oxide, activated carbon, and two types of hard coal. The study involved porous structure characterization using volumetric and microscopic techniques, measurements of hydrogen adsorption isotherms using the Sieverts apparatus and determination of the isosteric heat of adsorption. The highest adsorption capacities in relation to hydrogen were observed at low temperatures and low pressures, confirming that physisorption is the dominant adsorption mechanism in the investigated materials. Activated carbon and carbon nanotubes exhibited the highest adsorption capacities – up to 11.4 mmol/g and 3.3 mmol/g, respectively – demonstrating their potential for low-temperature hydrogen storage applications. In contrast, hard coals showed lower capacities, ranging from 0.9 mmol/g to 1.54 mmol/g. The isosteric heat of adsorption (Q_{st}) at the initial stages of adsorption varied between 6.5 kJ/mol and 13.2 kJ/mol, decreasing exponentially as surface coverage progressed. The greatest differences in heat distribution were observed in materials with strongly heterogeneous surface characteristics. For the coal samples, Q_{st} values ranged from 8.4 to 9.1 kJ/mol.

Keywords: Hydrogen storage; sorption capacity; heat of adsorption; carbon nanomaterials; hard coal

List of symbols

a [mmol/g] – is the equilibrium adsorption capacity at pressure p,
a_m [mmol/g] – is the total adsorption capacity at pressure $p \rightarrow \infty$,

[1] STRATA MECHANICS RESEARCH INSTITUTE, POLISH ACADEMY OF SCIENCES, 27 REYMONTA STR., 30-059 KRAKÓW, POLAND
[2] INSTITUTE OF METALLURGY AND MATERIALS SCIENCE, POLISH ACADEMY OF SCIENCES, 25 REYMONTA SYT., 30-059 KRAKÓW, POLAND
[3] AGH UNIVERSITY OF SCIENCE AND TECHNOLOGY, FACULTY OF GEOLOGY, GEOPHYSICS AND ENVIRONMENTAL PROTECTION, AL. MICKIEWICZA 30, 30-059 KRAKÓW, POLAND

* Corresponding author: pajdak@imgpan.pl

$A_0...A_n$; $B_0...B_n$ – are the best fit parameters;
AC – is activated carbon,
AIM – is adsorption isotherm analysis method,
b [1/MPa] – is the adsorption equilibrium constant related to the characteristic energy of the energy distribution function,
BET – is Brunauer-Emett-Teller model,
BJH – is Barrett-Joyner-Halenda model,
BSE – is backscattered electron,
c [–] – is the heterogeneity exponent ($0 < c \leq 1$), the smaller its value, the larger the width of the adsorption energy distribution; for $c = 1$ the isotherm takes the form of the Langmuir isotherm,
C [–] – is the adsorption equilibrium constant dependent on the difference between the heat of adsorption of the first layer and the heat of condensation,
CIM – is direct isothermal calorimetry method,
CNT – carbon nanotubes,
CNT15, CNT50 – are multi-walled carbon nanotubes with outer dimeter 8-15 and 30-50 respectively
DFT – is density functional theory,
GHG – is greenhouse gases,
GO – is graphene oxide,
IUPAC – is International Union of Pure and Applied Chemistry,
N [mol] – is the number of moles,
N_A [1/mol] – is the Avogadro's number,
L-F – is Langmuir-Freundlich isotherm,
oBC – is coal from the Budryk Coal Mine, classified as air-dried medium-rank Ortho-bituminous coal,
p [MPa] – is the absolute pressure,
p/p_0 [–] – is the relative pressure,
pBC – is coal from the Sobieski Coal Mine, classified as air-dried medium-rank Para-bituminous coal,
Q_{st} [kJ/mol] – is the isosteric heat of adsorption,
R [(J/mol)·K] – is the gas constant,
rGO – is reduced graphene oxide,
S [m^2/g] – is the specific surface area,
SE – is secondary electron detector,
SEM – is scanning electron microscopy method,
T [K] – is the temperature,
TEM – is transmission electron microscopy method,
ω [nm^2] – is the surface area occupied by a single adsorbate molecule in a monomolecular layer, the so- called sitting surface,
V [cm^3] – is the volume of the system,
Z [–] – is the gas compressibility coefficient (for an ideal gas $Z = 1$),
n, k – are the degrees of the polynomials approximating the functions appearing in the equation,
θ [–] – is the adsorbent surface coverage by adsorbate molecules (relative adsorption).

1. Introduction

Hydrogen technologies represent one of the most rapidly developing sectors in the energy industry. Hydrogen meets both environmental criteria – its combustion does not release greenhouse gases into the atmosphere [1-3] – and energy-related requirements, with an energy density of 143 MJ/kg [4]. It is also geopolitically and climatically independent. The main obstacle to the development of this technology is the storage of this product, which is strictly dependent on the direction of its use. For automotive needs, there are several possibilities for storing hydrogen: under high pressure, at low temperature (cryogenically) and accumulated in a solid state [5]. The use of hydrogen in fuel cells or combustion engines requires the development of an economical method of obtaining hydrogen, as well as its safe storage [2,6].

High-pressure hydrogen storage requires maintaining controlled pressure conditions (80 MPa) and high mechanical strength of the tanks. It is highly energy-intensive and dangerous during a vehicle collision. Low-temperature hydrogen storage is not suitable for automotive applications due to, among others, the high energy consumption necessary to liquefy the gas (33 K) [1]. On the other hand, storing hydrogen asorbed in the solid materials is a fairly promising method [7]. In this method, hydrogen reacts with a solid material as a result of chemical absorption, creating a new compound [8]. Another method is the accumulation of H_2 in polymers or metal alloys [9] and physical binding of H_2 to the surface of porous structures in physical adsorption [10-12]. Since storing hydrogen in the form adsorbed on the surface of a material, metal hydrides or intermetallic phases is a safe process, metal hydrides and carbon-based structures are the two main types of materials that have been the subject of much research over the last dozen or so years for their use as hydrogen storage materials [13-17].

Carbon materials are considered promising for hydrogen storage, e.g. in fuel cells due to the possibility of using them for both physisorption and chemisorption. Carbon materials of anthropogenic origin are extended structures designed for adsorption (activated carbons), or based on modern graphene systems, such as carbon nanotubes or graphene oxide. There are studies on their use as greenhouse gases (GHG) adsorbents [18,19]. Carbon nanomaterials have many advantages, including being easily available, thermally resistant and having a highly developed pore structure. Graphene oxide (GO) and carbon nanotubes (CNT) are popular and relatively easy to synthesize graphene compounds. Their hydrogen accumulation potential has been studied by many authors. According to [20] the efficiency of H_2 sorption by carbon nanomaterials is proportional to their BET surface area and micropore volume. Also according to Klechikov et al. [21] the adsorption capacity to hydrogen and pore structure in graphene nanomaterials are strongly correlated. This relationship is valid for many graphene compounds, especially those with a specific surface area up to 1000 m^2/g [22].

Temperature and pressure significantly influence the efficiency of hydrogen (H_2) accumulation [23]. At elevated pressures, both the specific surface area and sorption efficiency may decrease, primarily due to particle aggregation induced by hydrogen pressures exceeding 12 MPa. Typically, sorption capacities in relation to H_2 of these materials at room temperature (298 K) and a gas pressure of 10 MPa reach up to approximately 1 wt.%. At liquid nitrogen temperature (77 K), the maximum values increase substantially, ranging from about 4 to 7 wt.% [20,24]. Rajaura et al. [25] investigated the H_2 uptake capacity at room temperature (298 K) in pristine graphene oxide (GO) and its reduced form (rGO). The H_2 storage capacity in GO was 1.90 wt.%, while in rGO it decreased to 1.34 wt.%. Burres et al. [26] reported hydrogen uptake in the range of

1.0-1.2 wt.% for GO at 77-87 K under a pressure of 0.7 MPa. Similarly, Kim et al. [27] observed hydrogen capacities of 4.8 wt.% at 77 K and 0.49 wt.% at 298 K for GO under 9 MPa pressure. In a study by Aboutalebi [28], H_2 sorption efficiencies of 0.9 wt.% for carbon nanotubes (CNTs) and 1.4 wt.% for GO were obtained at 298 K and 0.5 MPa.

Hydrogen sorption performance can be further enhanced by decorating GO with metals such as boron, yttrium, silicon, or platinum nanoparticles [29-31]. According to Durgun et al. [32], functionalizing graphene with scandium, vanadium, and titanium allows for achieving high theoretical gravimetric hydrogen densities of 8.0, 7.5, and 7.8 wt.%, respectively. These values were experimentally supported by the findings of Mashoff et al. [33].

Naturally derived carbonaceous materials, including hard coals, are characterized by strong structural and chemical heterogeneity. The sorption capacity of hydrogen on hard coal is crucial for assessing its suitability as a hydrogen storage medium in geological coal formations. Current studies show that H_2 sorption on coal is possible, but its efficiency is low compared to other gases. Liu and Liu [34] conducted sorption and diffusion studies on various coals and determined the sorption capacity of H_2 in the range of 0.82-1.17 mmol/g at pressures of 0-6.5 MPa. Hydrogen is adsorbed on coal in significantly smaller quantities than CO_2 or CH_4, which is due to its small molecular size and weak interaction with the coal surface. This is confirmed by numerous studies, although the sorption efficiency of coal varies depending on the measurement conditions. Sayyafzadeh et al. [35] found that the sorption capacity of CO_2 on coal was seven times greater than that of H_2 at a pressure of 10 MPa. This difference in sorption efficiency is very high and may result from the applied measurement pressure. According to Czerw et al. [36], the sorption capacity of CO_2 and CH_4 at low pressure conditions (0-0.1 MPa) was 0.89 mmol/g and 0.13 mmol/g, respectively, while according to Skoczylas et al. [37] at preferential pressure (1.6 MPa) and temperature (278 K), it was 2.99 mmol/g and 1.25 mmol/g, respectively. These values are smaller or at most twice as large as the sorption capacity of H_2 investigated by Liu and Liu [34]. Coal exhibits selective sorption, preferring gases such as CO_2, which can be used for CO_2 separation and storage, but limits the efficiency of H_2 storage. The highest sorption capacity of H_2 is found in coals with high porosity and oxygen functional group content, but even in these cases the values are low [34,38]. Hydrogen, on the other hand, is characterized by better gas diffusivity in the coal matrix, defined by the effective hydrogen diffusivity. Effective hydrogen diffusivities in coal decrease with increasing pressure, with the lowest diffusivity being up to four times higher than for CH_4 [34]. High H_2 diffusivity in coal can be beneficial for rapid injection and extraction, although low sorption capacity limits the practical use of coal as an effective hydrogen storage medium.

The characterization of the gas sorption mechanism in hard coals usually focuses on their potential for the GHGs accumulation [37,39,40]. In the context of a comprehensive analysis of gas storage in such structures, in addition to the sorption capacity and kinetics parameters, thermodynamic aspects such as the heat of adsorption are increasingly taken into account [41,42]. The analysis of the thermodynamics of the sorption process allows for a better understanding of the mechanisms and energy transformations occurring on the coal surface. Moreover, the temperature effect accompanying the sorption process can significantly affect the local coal temperature [43,44].

Thermodynamic properties are also crucial for understanding the heat balance and mass transfer mechanisms in coal deposits [45]. The heat of adsorption reflects the strength of interactions between the sorbent and the sorbate and determines the amount of energy released or

absorbed during the adsorption of a unit amount of a substance, with a fixed degree of coverage of the adsorbent surface [46].

The isosteric heat of adsorption provides unique information on the intensity of the process, the type of adsorption and its course [45,47,48]. It is also an important thermodynamic parameter that describes the conversion of energy between the gaseous and adsorbed state. This parameter can be used to assess the adsorption capacity of coal, the energy inhomogeneity of its surface and temperature changes accompanying the adsorption and desorption processes, which directly affects the kinetics of these phenomena [49,50].

Various methods are used to assess the isosteric heat of adsorption, including: adsorption isotherm analysis method (AIM) and direct isothermal calorimetry (CIM) [51,52]. In the AIM method, energy dependence is determined based on the adsorption equilibrium points measured at different temperatures using the Clausius-Clapeyron equation.

This paper presents a comparative analysis of the structural, sorption and thermal properties of six carbon and coal structures: carbon nanotubes of different diameters (CNT15 and CNT50), reduced graphene oxide (rGO), activated carbon (AC) and two types of hard coal (pBC and oBC), in the context of their suitability as materials enabling controlled hydrogen accumulation. In order to determine the nature of changes in the adsorption capacity of carbon structures with respect to H_2, a limiting pressure value was also determined, after which the change in the adsorption capacity value becomes independent of pressure and in some cases also independent of the process temperature. For each materials, the isosteric heat of adsorption was also determined and compared as a function of the degree of surface filling. The heat of adsorption values were determined for adsorption capacities at several temperatures and at pressures of 20 kPa.

2. Research methodology

The surface topography and phase changes of carbon structures were characterized by scanning electron microscopy (SEM). A Philips XL30 electron microscope equipped with a secondary electron (SE) detector and a backscattered electron (BSE) detector was used. Analyses were performed in high-pressure mode. Before measurement, samples were silver-sputtered and images were recorded at magnifications from 100× to 5000×, with an electron beam with an accelerating voltage of 8 kV. Precise contrast analysis of the microstructure of the materials was performed using transmission electron microscopy (TEM) on an FEI Technai G2 analyzer.

The structural studies of the pore space of the materials were performed by the low-pressure gas adsorption method, using the ASAP 2020 analyzer (Micromeritics). According to the manufacturer's data, this analyzer has a measurement expanded uncertainty in the amount of adsorbed substance in the range of 1-2%. Nitrogen (N_2) in the gas phase was used as the adsorbate at a temperature of 77 K. Based on the volumetric method, the volume of adsorbed gas was recorded as a function of pressure 0-0.1 MPa ($0 < p/p_0 < 0.996$). Based on the sorption equilibrium points, adsorption and desorption isotherms were plotted, and structural parameters were determined on their basis. Depending on the type of material, the specific surface area was determined according to the monolayer Langmuir model (1,2) or the multilayer Brunauer-Emett-Teller (BET) model (3):

$$\theta = \frac{bp}{1+bp} \tag{1}$$

where:

$$\theta = \frac{a}{a_m} \tag{2}$$

$$a = \frac{a_m C\, p / p_0}{\left(1 - p / p_0\right)\left[1 + \left(C - 1\right) p / p_0\right]} \tag{3}$$

Taking into account the so-called sitting surface of the sorbate particle, the specific surface area of the materials is determined using equation:

$$S = a_m \omega N_A \tag{4}$$

The IMI-HTP sorption analyzer (Hiden Isochema) was used for sorption measurements of hydrogen, which is based on the Sieverts volumetric method. According to the manufacturer's data, it has a measurement uncertainty of 2%. This method is based on the gas state Eq. (5), in which the pressure is proportional to the number of moles of gas:

$$p_V = NZRT \tag{5}$$

Assuming that p, V, Z, R, T are constant values, it is possible to determine the number of moles of hydrogen adsorbed or desorbed:

$$\Delta N = \frac{p_1 V_1}{ZRT} - \frac{p_2 (V_1 + V_2)}{ZRT} \tag{6}$$

In the volumetric Sieverts method, the volume of the reference chamber V_1, which is maintained at a constant temperature, and the volume of the reactor V_2, which contains the sample, are measured. During the sorption measurement, a predefined pressure is applied to volume V_1 while the reactor valve remains closed. Once the equilibrium pressure p_1 is reached, this value is recorded. To determine the pressure p_2, the valve to the reactor containing the sample is opened, and the system is allowed to reach a new equilibrium pressure.

Hydrogen sorption measurements on carbon and coal structures began with an activation process. The sample was heated under vacuum at a temperature of 373 K for 2 hours and then cooled to ambient temperature. Subsequently, the samples were examined in the low-temperature range (81-173 K) as well as in the high-temperature range (373-573 K). The obtained sorption data points were fitted using Langmuir-Freundlich (L-F) isotherms:

$$a = \frac{a_m \left(bp\right)^c}{1 + \left(bp\right)^c} \tag{7}$$

In order to observe the changes in the adsorption capacity values with respect to H_2 on carbon and coal structures, the derivative of the Langmuir-Freundlich sorption isotherm function was used $(da)/(dp)$:

$$\frac{da}{dp} = \frac{a_m bc \left(bp\right)^{c-1}}{\left(1 + \left(bp\right)^c\right)^2} \tag{8}$$

In order to determine the thermal effects accompanying hydrogen sorption, calculations of the isosteric heat of adsorption were performed using the adsorption isotherm method (AIM). Sorption isotherms were fitted to the hydrogen adsorption equilibrium points determined at several temperatures using the L-F model (Eq. (7)) and an isostere plot was constructed. The isosteric heat of adsorption was calculated from the isostere angle presented in the coordinate system (9) for a specific amount of adsorbed hydrogen. The differential form of the Clausius-Clapeyron Eq. (10) [53] was used, and the detailed Eq. (11) was used for numerical calculations:

$$\ln p = f\left(\frac{1}{T}\right) \tag{9}$$

$$\left(\frac{\Delta \ln p}{\Delta \frac{1}{T}}\right) = \frac{-Q_{st}}{R} \tag{10}$$

$$\ln p = \frac{1}{T}\sum_{i=0}^{n} A_i v^i + \sum_{i=0}^{k} B_i v^i + z \ln v \tag{11}$$

The isosteric heat of adsorption as a function of surface coverage was calculated using equation:

$$Q_{st}(v) = -R\left(\frac{\partial \ln p}{\partial\left(\frac{1}{T}\right)}\right)_v = -R\sum_{i=0}^{n} A_i v^i \tag{12}$$

3. Research material

Five types of carbon materials with different physicochemical structures were used to study the efficiency of hydrogen accumulation. Groups of homogeneous carbon structures (carbon nanotubes, reduced graphene oxide, activated carbon) and highly heterogeneous natural carbon materials (hard coals) were selected for the study.

The study included two types of multi-walled carbon nanotubes (CNT15, CNT50) manufactured by Nanostructured & Amorphous Materials, Inc., which were produced by the Catalytic CVD method. In TABLE 1 are shown parameters specified by the producer. The tested CNTs had a carbon (C) content of 97.4%, chlorine (Cl) of 0.2%, iron (Fe) of 0.5%, nickel (Ni) of 1.9% and a trace content of sulfur (S).

The images taken using the TEM method (Fig. 2) show CNTs in the bright field (BF) (Fig. 1A,B) and the high-resolution HREM microstructure (Fig. 1C,D). The observed CNTs, regardless of their type, were unevenly arranged, tangled and bent. Their external surface showed irregularities and the walls were not continuous in some places and had structural defects. The structure of CNT walls showed correctly arranged concentric graphene layers and fullerene ends.

TABLE 1

Carbon nanotube (CNT) parameters

Symbol	Outer dimeter	Inner diameter	Length	Density	Purity
Unit	nm	nm	μm	g/cm^3	%
CNT15	8-15	3-5	10-50	2.3	>95
CNT50	30-50	8-15	10-20		

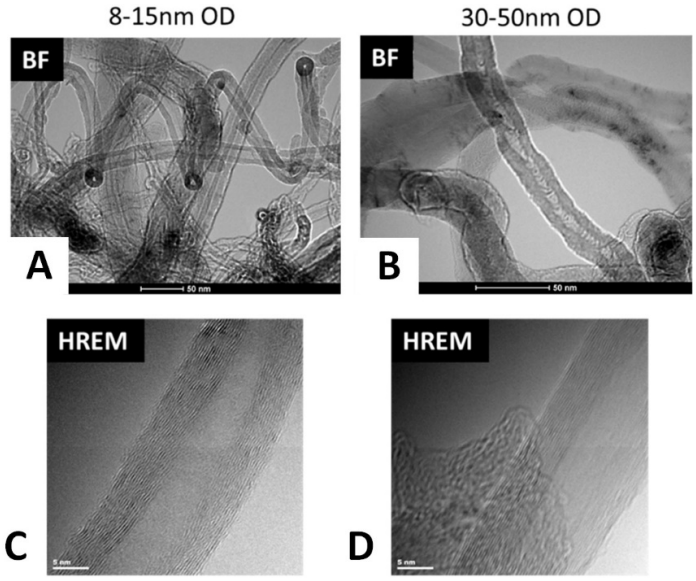

Fig. 1. TEM images of carbon nanotubes CNT, A) bright field image of CNT15, B) bright field image of CNT50, C) high resolution image of CNT15, D) high resolution image of CNT50

Reduced graphene oxide (rGO) was synthesized using a modified Hummers method at the Institute of Electronic Materials Technology in Warsaw. According to the producer's data, the rGO tested contained carbon (C) at a level of 70-80%, oxygen (O) at a level of 15-20%, and sulfur (S), hydrogen (H) and nitrogen (N) below 2%, which are the elements involved in the synthesis of rGO. SEM images (Fig. 2) show sheets with diameters in the range of 5-30 μm and thickness of graphene layers of about 0.5 μm. The use of graphene oxide reduction is aimed at increasing its surface area, especially using post-synthesis activation procedures. Causing a large number of defects, including discontinuities and pores in the graphene sheets, allows obtaining rGO with a highly developed surface [54].

Activated carbon AC is a highly porous variety of carbon, characterized by an expanded pore space, which can make it an exceptionally effective adsorbent. CARBO VP activated carbon was used in the study, which is a commercial product made from carbon raw materials or other materials of organic origin. The SEM images show the structure of the tested AC, which is heterogeneous and disordered (Fig. 3). The AC particles are of different sizes with a lamellar structure and different particle sizes.

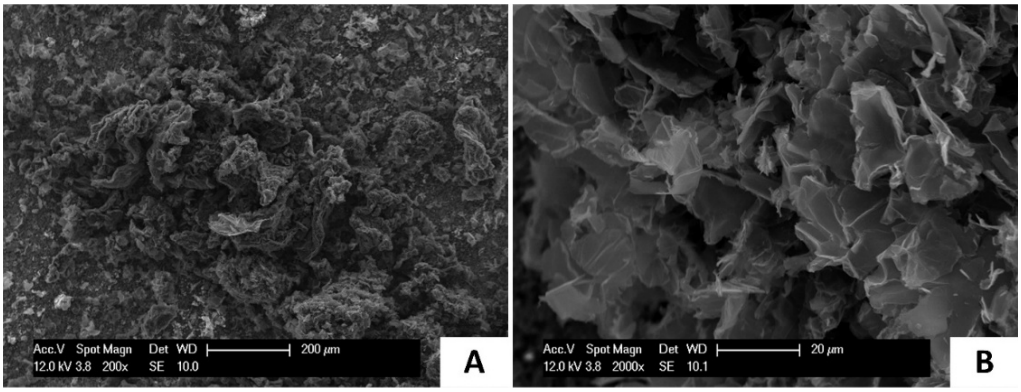

Fig. 2. SEM images of reduced graphene oxide rGO, A) 200× magnification, B) 2000× magnification

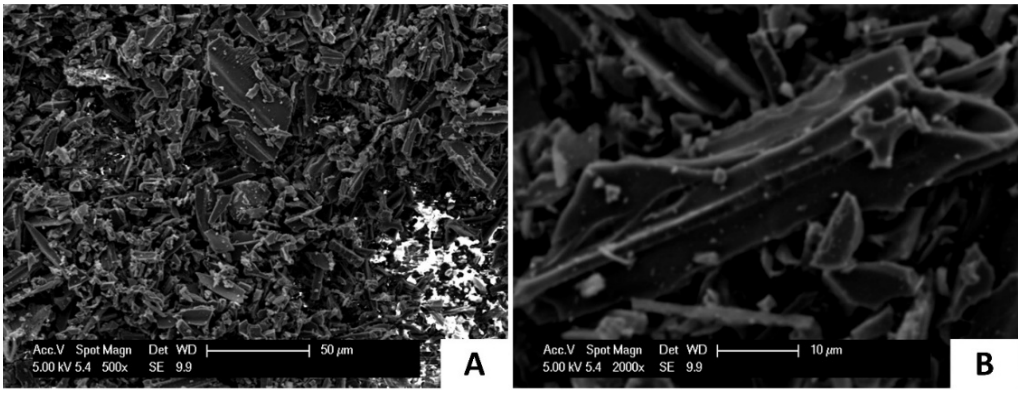

Fig. 3. SEM images of activated carbon AC, A) 500× magnification, B) 2000× magnification

The two types of hard coal used for the study differed significantly in composition and petrographic parameters. They came from Polish mines: Sobieski Coal Mine (pBC) and Budryk Coal Mine (oBC). The pBC coal from the Sobieski Coal Mine is mined from a depth of about 500-700 m below the surface. According to the UN-ECE International Classification of In-Seam Coal [55], it is classified as air-dried medium-rank Para-bituminous coal. It has a vitrinite reflectivity of 0.54% and 73% vitrinite in the maceral composition [19]. SEM images (Fig. 4) show that the grains of the pBC sample have sharp edges, the color of the grains is uniform and intensely dark, which confirms the high content of vitrinite maceral (73%).

The oBC coal from the Budryk Coal Mine is mined from a depth of about 1300 m below the surface. It has been classified as air-dried medium-rank Ortho-bituminous coal. The reflectivity of vitrinite here was 0.95%, which is confirmed by SEM images (Fig. 5) where the surface of the sample reflects some light. The oBC sample has a lower content of vitrinite maceral equal to 63%, a smooth surface without visible pores, but the structure contains elements of other macerals, including inertinite [19].

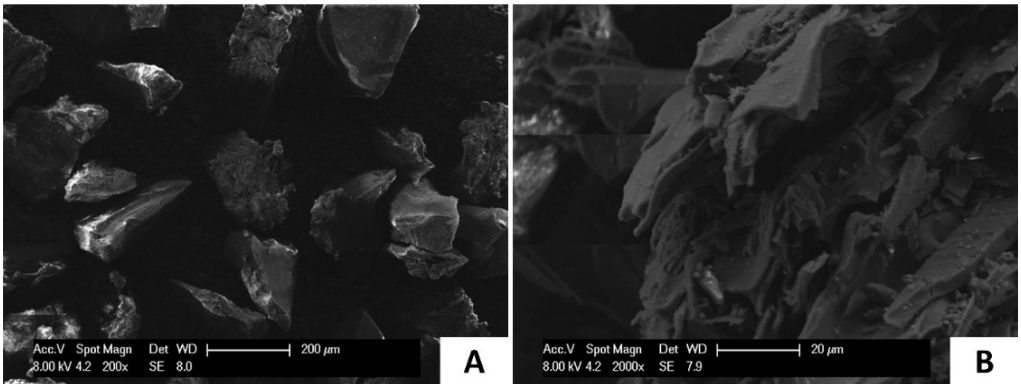

Fig. 4. SEM images of medium-rank Para-bituminous coal pBC, A) 200× magnification, B) 2000×x magnification

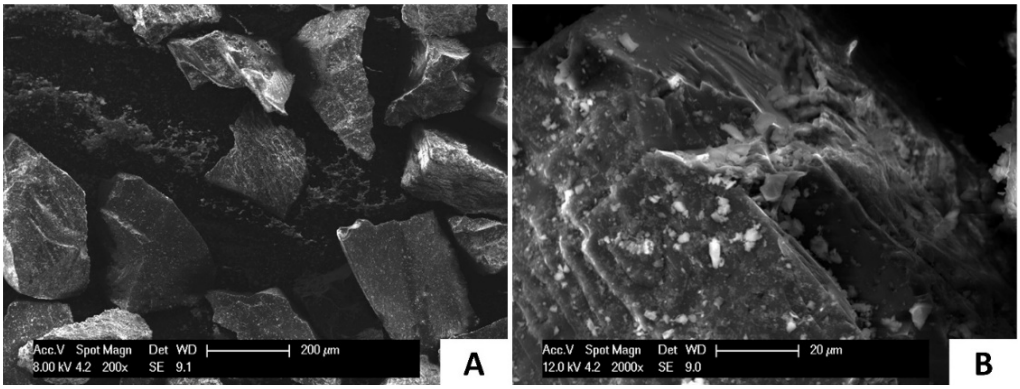

Fig. 5. SEM images of medium-rank Ortho-bituminous coal oBC, A) 200× magnification, B) 2000× magnification

4. Results and discusion

4.1. Surface pore structure

The studies were performed using the low-pressure gas adsorption method (section 2). In all materials, the course of equilibrium sorption points at pressure of 0-0.1 MPa had the shape of the type III isotherm according to the IUPAC system, which is characteristic for mesoporous and weakly porous materials. Since carbon and coal structures are structurally different, the measured values of sorption capacities were significantly different from each other (Fig. 6). Sorption capacity increased evenly in the pressure range of 0-0.8 MPa (CNT, rGO) and in the range of 0-0.9 MPa (AC), while above these pressure ranges, adsorption on the surface intensified without showing a clear plateau at the saturation stage. The total sorption capacity in CNT15 and CNT50 was 508 cm^3/g and 240 cm^3/g, respectively (Fig. 6A). As a result of

desorption in CNTs, H3 type adsorption/desorption hysteresis was obtained, the shape of which indicates an irregular structure of slit pores. This type of hysteresis occurs in carbon materials containing aggregates of plate-like particles, such as porous carbon materials, graphite, some clays and aerogels. In the tested CNTs, which are chemically homogeneous materials, the shape of hysteresis reflects gas desorption, which is delayed and occurs not only in the CNT carbon matrix but also between single graphene layers. In rGO and AC, the final increase in adsorption intensity results from the capillary condensation effect and the total sorption capacity was 90 cm^3/g (rGO) and 69 cm^3/g (AC). As a result of N_2 desorption, H4 type hysteresis was obtained in both cases, characteristic for microporous and mesoporous materials (Fig. 6B). The pore emptying mechanism was significantly delayed. The hysteresis loop curvature occurred in the pressure range of 0.4-0.6 MPa, which is the effect of adsorption in smaller slit pores with simultaneous capillary condensation in mesopores. The diversification of porosity should be seen in the heterogeneity of the porous structure of these materials. Both materials have an extensive system of pores with different diameters. In hard coals (Fig. 6B), N_2 adsorption was at a typical low level for these materials and no hysteresis loop was observed here. The maximum sorption capacity achieved at a pressure of about 0.1 MPa was 31 cm^3/g for pBC, while for oBC it was below 2 cm^3/g.

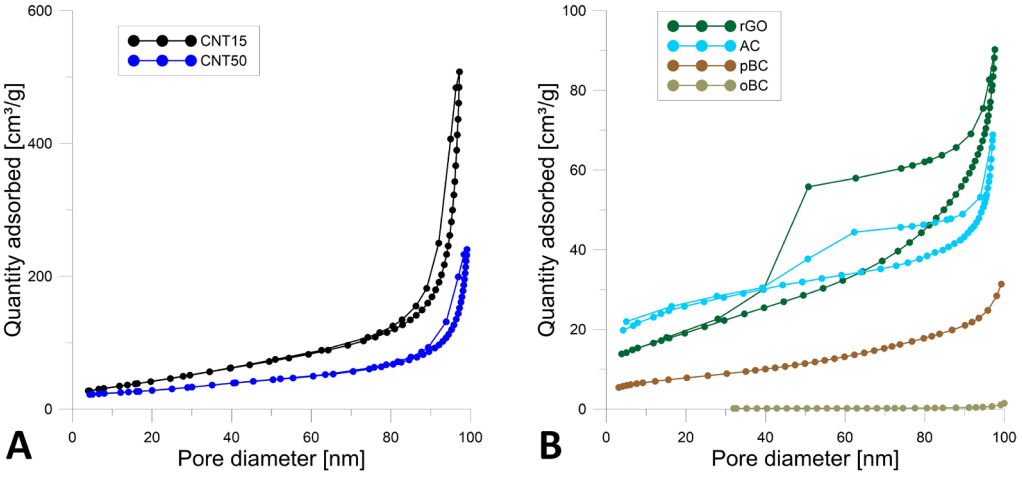

Fig. 6. Nitrogen adsorption isotherms, A) CNT15, CNT50, B) rGO, AC, pBC, oBC

Based on the measurement data and formulas (section 2), the structural parameters of carbon materials were determined (TABLE 2).

Tested materials had different values of structural parameters, with carbon nanotubes having the most intensively developed pore volume and specific surface area. Its value assuming the multilayer BET model was higher for CNT15 and amounted to 166 m^2/g, and in CNT50 103 m^2/g, respectively. Assuming a monolayer surface coverage with adsorbate, the Langmuir specific surface area was at a much higher level and amounted to 517 m^2/g (CNT15) and 260 m^2/g (CNT50). The volume of pore space in CNT15 was similar for mesopores and micropores and amounted to about 0.7 cm^3/g, and the predominant volume share was pores with a diameter of

TABLE 2

Parameters of carbon and coal structures

Sample	Adsorption capacity at 0.1 MPa	Surface area		Pore volume		Average pore size
Used model		BET	Langmuir	BJH (Mesopore volume)	DFT (Micropore volume)	BET
Unit		m^2/g	m^2/g	cm^3/g	cm^3/g	nm
rGO	90.26	64.56	179.04	0.139	0.072	7.5
CNT15	508.02	166.36	517.44	0.749	0.718	15.0
CNT50	240.52	102.61	260.75	0.363	0.268	12.8
AC	68.83	87.12	162.50	0.097	0.052	5.5
pBC	31.37	27.42	68.06	0.041	0.046	9.4
oBC	1.46	0.36	1.49	0.002	0.001	29.7

1.5-4 nm (Fig. 7). In CNT50, the pores had a volume in the range of 0.26-0.36 cm^3/g and the largest volume share in the range of 2-4 nm (Fig. 7). Similar structural parameters were determined in rGO and AC. These materials had a BET specific surface area in the range of 64-87 m^2/g, while the Langmuir surface area was in the range of 162-179 m^2/g, respectively. They had a more developed mesopore volume and ranged from 0.10 cm^3/g to 0.14 cm^3/g. The pore size distribution was most developed in pores with a diameter of 2-3 nm. In natural carbon materials – hard coals, the specific surface area value was strictly dependent on the type of coal. In the pBC coal, the measured BET and Langmuir specific surface areas were 27 m^2/g and 68 m^2/g, respectively, while in oBC they were below 2 m^2/g. The pore volume in pBC was below 0.05 cm^3/g, while in pBC they were on the margin of error. In coals with low vitrinite reflectivity and high vitrinite maceral content, the smallest pores, the so-called ultramicropores, which are difficult to study using N_2 and give much lower results. To avoid these ambiguities, CO_2 is used for measurements as an alternative [19].

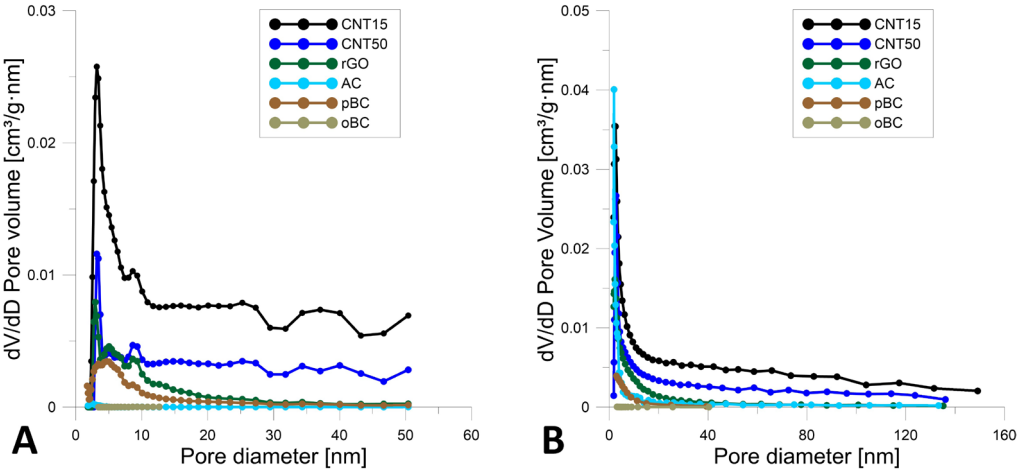

Fig. 7. Pore size distribution, A) according to DFT model, B) according to BJH model

4.2. Hydrogen sorption efficiency

Based on the sorption equilibrium points, hydrogen (H_2) sorption isotherms were determined for the analyzed samples. Considering that both carbon nanomaterials and hard coal are structurally composed primarily of micropores and small mesopores [12,56], it was assumed that the pore sizes in these materials are comparable to the diameter of hydrogen molecules. As a result, monolayer coverage of the sorbent surface occurs, which justifies the application of the Langmuir-Freundlich sorption model (Eq. (7)) to describe the sorption processes. This model demonstrated very good agreement with the experimental data. The efficiency of hydrogen adsorption in carbon and coal structures was directly proportional to the pressure and inversely proportional to the temperature.

H_2 sorption measurements on carbon structures (rGO, CNT15, CNT50 and AC) were performed at 4-5 temperatures for absolute pressure from 0 to 3000 kPa. The most effective surface coverage by hydrogen occurred at low pressure ranges. In carbon nanotubes with a smaller diameter of CNT15 tubes, the H_2 sorption efficiency ranged from 0.8 to 3.3 mmol/g (Fig. 8a), while in CNT50 it was in the range of 0.5-2.2 mmol/g (Fig. 9a). In reduced graphene oxide, a similar H_2 sorption efficiency was achieved as in CNT50. The sorption capacity with respect to H_2 at the maximum measurement pressure ranged from 0.5 to 2.8 mmol/g (Fig. 10a). The highest value of this parameter was obtained in AC and it was in the range of 0.5-11.4 mmol/g (Fig. 11a). In all samples the hydrogen sorption efficiency was strictly dependent on the temperature at which the process was carried out. The highest sorption efficiency was achieved at 123 K.

In order to determine the nature of changes in the sorption capacity of carbon structures in relation to H_2, the derivative of the Langmuir-Freundlich sorption isotherm (Eq. (8)) was determined. At all tested measurement temperatures for carbon materials, the coefficient of determination R^2 was in the range of 0.995-0.999. This adjustment allowed for the identification of the pressure value, beyond which the change in the sorption capacity value in carbon and coal structures becomes independent of pressure and, in some cases, also independent of temperature. With increasing pressure, the derivative curves at different temperatures tended to flatten, indicating a gradual saturation of available sorption sites on the material surface. This flattening suggests that at higher pressures the rate of increase of sorption capacity in relation to pressure decreases, reflecting the approach to the monolayer adsorption limit. Furthermore, the convergence of derivative values at different temperatures suggests that the increase in temperature reduces the adsorption. This may result from the saturation of the most energetically favorable micropores, after which adsorption occurs in less selective sites.

In the case of CNT15, the hydrogen sorption efficiency curves flattened (Fig. 8B). A plateau was reached at 20 MPa, except for the sorption curve at 123 K, where the plateau did not occurre at 20 MPa. The difference between the incremental changes in sorption capacity (*da*) at that point was $5.49 \cdot 10^{-5}$ mmol/(g·kPa). For CNT50, the dynamics of sorption capacity to hydrogen changes were more varied (Fig. 9B). The sorption processes at 123 K and 173 K were the most pressure-dependent. Additionally, at 573 K, an initial increase in sorption capacity was observed, although the magnitude of these changes was small and negligible in the context of the overall sorption rate. At 20 MPa, the difference in incremental values reached $1.22 \cdot 10^{-4}$ mmol/(g·kPa), indicating that temperature still had a significant effect on the sorption process in CNT50.

For rGO, the hydrogen sorption process at 123 K was the most pressure- dependent, and conditions approaching a plateau were reached at approximately 20 MPa (Fig. 10B). At this pressure, the difference in the derivative values across different temperatures was $9.77 \cdot 10^{-5}$ mmol/(g·kPa).

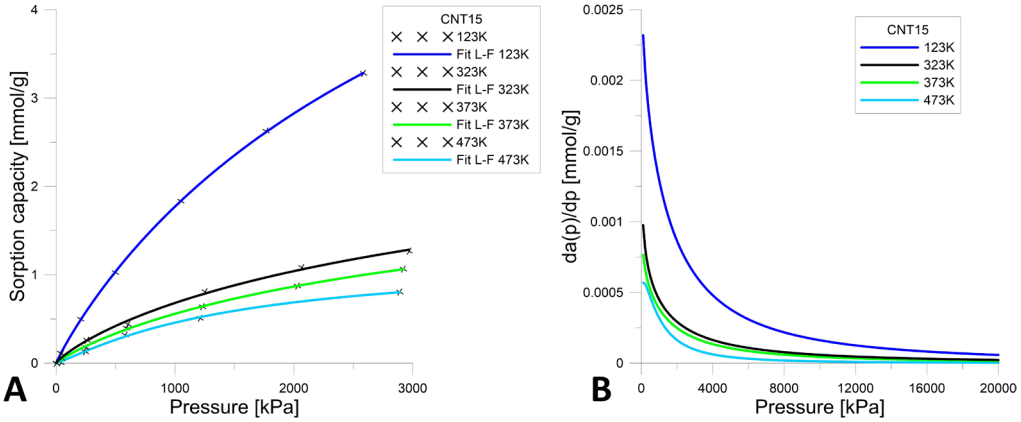

Fig. 8. Hydrogen adsorption on carbon nanotubes CNT15, A) H_2 adsorption isotherms (Langmuir-Freundlich model), B) elemental increase of H_2 adsorption

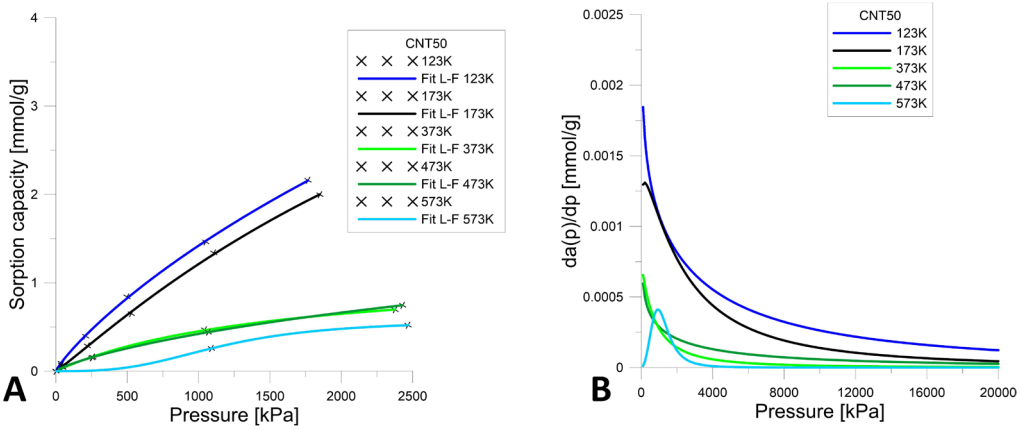

Fig. 9. Hydrogen adsorption on carbon nanotubes CNT50, A) H_2 adsorption isotherms (Langmuir-Freundlich model), B) elemental increase of H_2 adsorption

In the case of activated carbon (AC), the curves showed similar trends, and equilibrium was reached as early as 8 MPa (Fig. 11B). Increasing the pressure beyond this critical value did not lead to further increases in sorption capacity. Above this pressure, sorption efficiency was also independent of temperature.

The hydrogen sorption efficiency on coal structures (pBC and oBC) was evaluated at three temperatures and pressures up to 2400 kPa. Due to significant structural differences between the studied coals, their sorption capacities to hydrogen varied accordingly. The highest sorption capacities were observed at low pressures and at temperatures of 123 K and 173 K. In the highly microporous coal pBC, the maximum sorption capacity to H_2 ranged from 0.75 to 1.54 mmol/g at 123 K and 173 K, while at 373 K it dropped below 0.1 mmol/g (Fig. 12A). In contrast, hydrogen sorption on oBC coal, which has a higher proportion of mesopores in its pore structure,

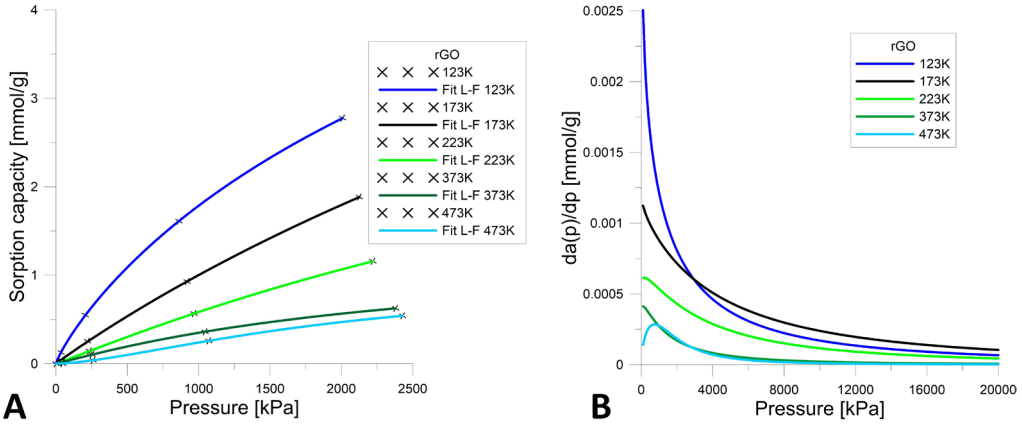

Fig. 10. Hydrogen adsorption on reduced graphene oxide rGO, A) H_2 adsorption isotherms (Langmuir-Freundlich model), B) elemental increase of H_2 adsorption

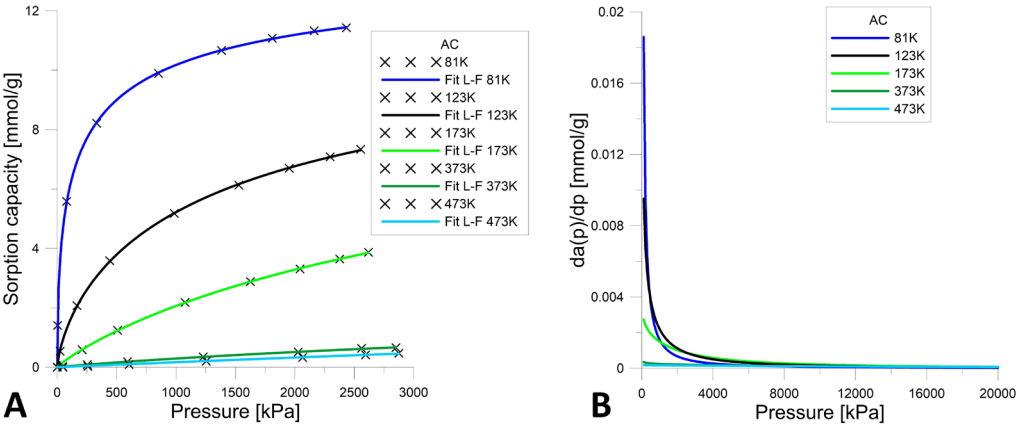

Fig. 11. Hydrogen adsorption on activated carbon AC, A) H_2 adsorption isotherms (Langmuir-Freundlich model), B) elemental increase of H_2 adsorption

reached 0.75 mmol/g and 0.90 mmol/g at 123 K and 173 K, respectively, and 0.15 mmol/g at 373 K (fig. 13A).

The variation in sorption capacity to hydrogen was determined up to a pressure of 20 MPa, based on the derivative of the Langmuir0Freundlich isotherm (Eq. (8)). The coefficient of determination R^2 for both hard coals was in the range of 0.995-0.999. The sorption capacity curves recorded at different temperatures exhibited a characteristic flattening trend as pressure increased (Figs. 12B and 13B), which reflects the progressive saturation of available adsorption sites within the porous structures of the coal samples. At the lowest measurement temperature of 123 K, the pressure had the greatest influence on both coal types, and this effect decreased with increasing measurement temperature. As the temperature increased to 173 K and 373 K, the influence of pressure on sorption efficiency decreased, which is consistent with the thermally driven reduc-

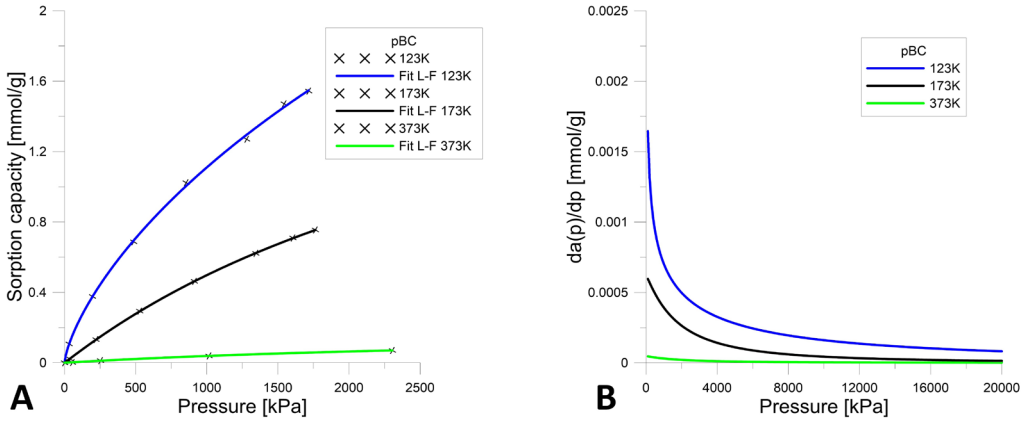

Fig. 12. Hydrogen adsorption on hard coal pBC, A) H_2 adsorption isotherms (Langmuir-Freundlich model), B) elemental increase of H_2 adsorption

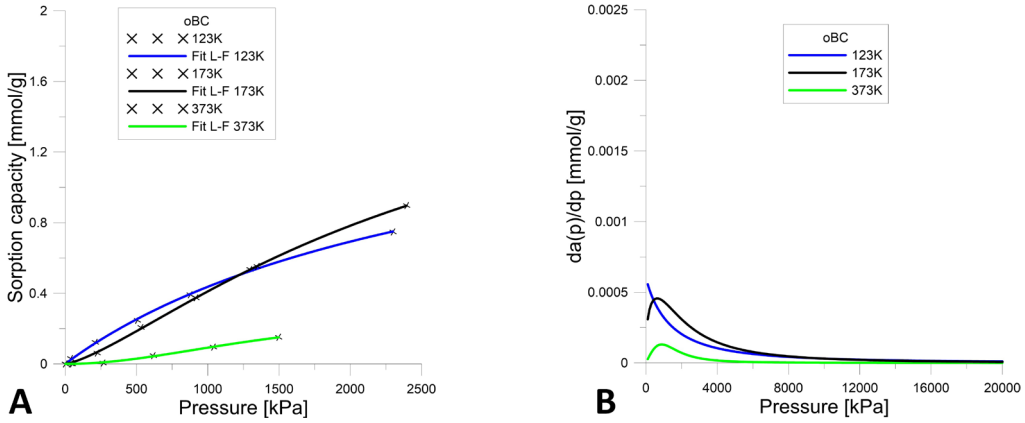

Fig. 13. Hydrogen adsorption on hard coal oBC, A) H_2 adsorption isotherms (Langmuir-Freundlich model), B) elemental increase of H_2 adsorption

tion in adsorption affinity. At approximately 20 MPa, the difference in the derivative values was $8.07 \cdot 10^{-5}$ mmol/(g · kPa) for pBC and $9.63 \cdot 10^{-6}$ mmol/(g · kPa) for oBC. These values indicate that at this high pressure, further increases in pressure result in minimal changes in sorption capacity. This flattening of the derivative curve suggests that the systems are approaching or have already reached equilibrium, with most accessible adsorption sites occupied. Therefore, the sorption process becomes largely independent of further pressure increases and, to a lesser extent, of temperature. Notably, the derivative value for pBC was an order of magnitude greater than that for oBC. This significant difference underscores the much higher pressure sensitivity of hydrogen sorption in pBC.

These findings highlight the critical role of pore size distribution and surface characteristics in governing the sorption behavior of hydrogen in coal-based materials and support the use of high-resolution isothermal analysis combined with derivative interpretation for evaluating sorbent performance under varying thermodynamic conditions.

4.3. Thermal effects of hydrogen adsorption

For each carbon and coal structure, the isosteric heat of adsorption (Q_{st}) was determined (section 2) and compared as a function of the surface filling degree. The heat of adsorption values were determined for sorption capacities at several temperatures and pressures of 20 kPa. Adsorption, understood here as a reduction in the number of degrees of freedom of hydrogen molecules located near the sorbent surface [57,58]. The process defined in this way occurs almost immediately and is accompanied by the release of a specific amount of heat. The amount of heat released during the attachment of hydrogen molecules to the surface of carbon and coal structures while maintaining a constant amount of adsorbed hydrogen was the highest in the initial stages of sorption. Then the surface of the materials was free from sorbate. This is due to the fact that at the beginning, hydrogen adsorbs on the strongest binding sites, and as adsorption progresses, it occupies increasingly weaker sorption sites. In all tested materials, a low Q_{st} value below 15 kJ/mol was obtained, which indicates a physical adsorption process accompanied by weaker, reversible interactions.

In CNT15 carbon nanotubes, at the initial stage of H_2 adsorption, the Q_{st} value was 13.2 kJ/mol (Fig. 14A). As the surface was filled with adsorbate, the heat of adsorption decreased exponentially up to a sorption capacity of 0.4 mmol/g, where it reached a minimum of 4.8 kJ/mol. Strong surface heterogeneity was observed here, which was manifested in a successive increase in the Q_{st} value up to 5.7 kJ/mol. In CNT50, a different course of the heat of adsorption parameter was obtained (Fig. 14B). The initial Q_{st} value was lower than in CNT15 and amounted to 7.9 kJ/mol. As the surface was filled with adsorbate, the heat exponentially

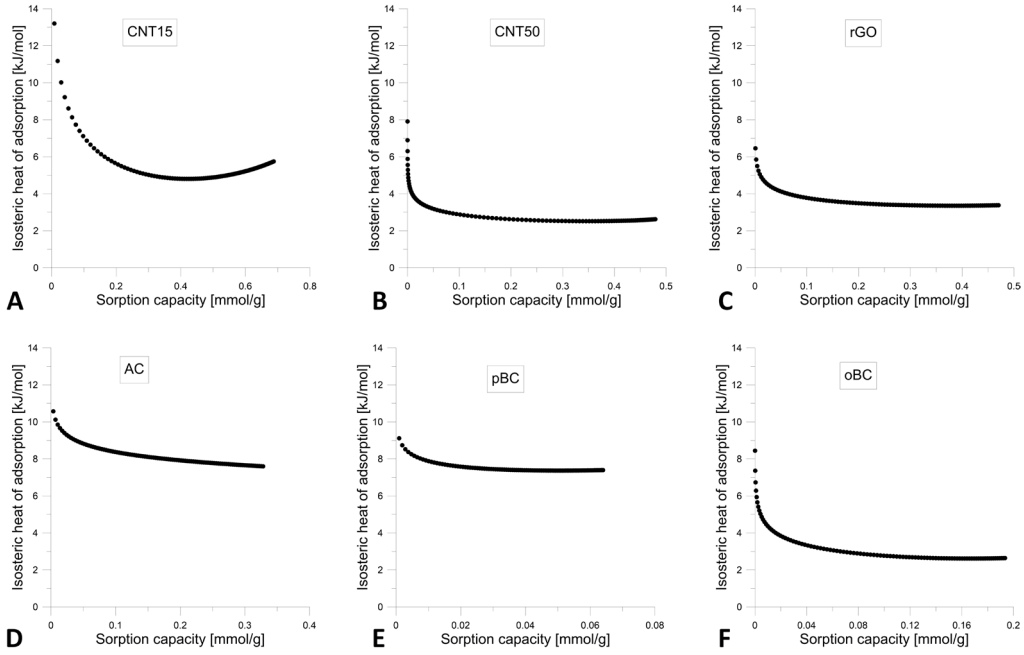

Fig. 14. Isosteric heat of adsorption, A) CNT15, B) CNT50, C) rGO, D) AC, E) pBC, F) oBC

decreased up to a sorption capacity of 0.2 mmol/g, after which the function graph became flat. The analysis of the course of Qst changes shows that CNT50 has a more homogeneous surface than CNT15, although the thermal effects accompanying hydrogen adsorption are smaller here. In the reduced graphene oxide, the value of the isosteric heat of adsorption (Q_{st}) changed with the filling of the surface with hydrogen molecules (Fig. 14C). The maximum value of Q_{st} at the beginning of the process was 6.5 kJ/mol. Up to the sorption value of 0.1 mmol/g, the heat of adsorption decreased its value, down to about 3.7 kJ/mol. The decrease in the Q_{st} value began to stabilize, which indicates the homogeneity of the rGO surface. At the end of adsorption at the highest measurement temperature (473K) and in the sorption capacity to H_2 of about 0.5 mmol/g, the value of the heat of adsorption was about 3.4 kJ/mol. The graph of changes in the isosteric heat of adsorption in AC was different from the others. In the initial stage of the process Q_{st} reached a maximum of 10.6 kJ/mol and then gradually decreased. Importantly, with the increase in the surface filling with sorbate, a plateau was not reached, and the Q_{st} graph was inclined towards the X axis and had an almost linear course. In pBC and oBC coals, the maximum heat of adsorption was 9.1 kJ/mol and 8.4 kJ/mol, respectively. These values decreased exponentially with the surface filling with adsorbate up to about 0.4 mmol/g (pBC) and 0.15 mmol/g (oBC). After this stage, the graph of Q_{st} changes reached a plateau and there were not observed further changes in this parameter.

5. Conclusions

The tested carbon and coal structures differed significantly in terms of structure. The obtained results indicate that nanocarbon materials (CNT and rGO) are characterized by a much more developed porous structure than natural carbons, which directly translated into higher sorption capacities in relation to hydrogen. Among them, the CNT15 sample showed the largest specific surface area (BET: 166 m^2/g; Langmuir: 517m^2/g), which correlated with the highest isosteric adsorption heat Q_{st} in the initial stage of the process (13.2 kJ/mol). Such a high Q_{st} value indicates the presence of sorption sites with strong potential for hydrogen binding, which makes this material particularly attractive in the context of applications at low temperatures and pressures. Compared to CNT15, the CNT50 material was characterized by a smaller specific surface area (BET: 103 m^2/g) and a lower initial Q_{st} (7.9 kJ/mol). Nevertheless, the Q_{st} evolution plot suggests a higher surface homogeneity, which may be beneficial from the point of view of thermal stability during cyclic adsorption–desorption processes.

Reduced graphene oxide (rGO) showed moderate textural parameters, however, low surface heterogeneity and stable Q_{st} values (max. 6.5 kJ/mol and final: 3.4 kJ/mol) suggest its potential utility as a lightweight and homogeneous sorbent under moderate pressure and temperature conditions. The highest sorption capacity to hydrogen was obtained for activated carbon (AC), where the maximum value reached 11.4 mmol/g. The Q_{st} value of AC was lower than that of CNT, but showed a linear decrease without reaching a plateau. This indicates a wide range of available sorption sites over the entire hydrogen saturation range of the material, which makes AC a very attractive material for buffer or stationary hydrogen storage, especially where volumetric capacity and material cost are important.

The pBC hard coal, despite its limited specific surface area (27 m^2/g), showed relatively high initial Q_{st} values (9.1 kJ/mol), which was attributed to the presence of ultramicropores inacces-

sible to nitrogen in conventional BET measurements. This indicates the need to use alternative methods (e.g. CO_2 adsorption) for a more complete characterization of porosity. On the other hand, the oBC sample, containing a higher share of mesopores, showed a lower and less stable sorption capacity, as well as lower Q_{st} values (max. 8.4 kJ/mol), which limits its application potential in the field of hydrogen storage.

In all the materials tested, the hydrogen sorption process was of a physical nature, as indicated by Q_{st} values below 15 kJ/mol and the dependence of the process efficiency on temperature and pressure. Adsorption occurred most intensively in the low pressure range and at a temperature of 123 K, which is typical for physisorption on microporous sorbents.

In summary, the greatest application potential as hydrogen sorbents was demonstrated by CNT15 nanotubes and activated carbon AC. The first material offers high binding energy, while AC combines high sorption capacity with technological and economic availability, which makes it particularly promising for hydrogen storage technology on a larger scale.

References

[1] L. Schlapbach, A. Zuttel, Hydrogen-storage materials for mobile applications. Nature **414** (6861), 353-8 (2001). DOI: https://doi.org/10.1038/35104634

[2] P. Singh, D. Balasubramanian, I.P. Venugopal, V.V. Tyagi, V. Goel, M. Wae-Hayee, M.A. Kalam, E.G. Varuvel, A comprehensive review on the applicability of hydrogen and natural gas as gaseous fuel for dual fuel engine operation. Energy Sources, Part A: Recovery, Utilization, and Environmental Effects **46** (1), 1559-1587 (2024). DOI: https://doi.org/10.1080/15567036.2023.2298004

[3] P.V. Sukumaran, Geological Hydrogen: A New Carbon-free, Clean Energy Vector. Journal of Geological Society of India **100** (3), 447-450 (2024). DOI: https://doi.org/https://doi.org/10.17491/jgsi/2024/173852

[4] S. Daghighi, P.M. Weaver, Nonconventional low-steered pressure vessels for hydrogen storage. Composite Structures 334, 117970 (2024) DOI: https://doi.org/10.1016/j.compstruct.2024.117970

[5] M. Fichtner, Nanotechnological aspects in materials for hydrogen storage. Adv. Eng. Mater. **7** (6), 443-55 (2005). DOI: https://doi.org/10.1002/adem.200500022

[6] M.R. Soltanian, A. Bemani, F. Moeini, R. Ershadnia, Z. Yang, Z. Du, H. Yin, Z. Dai, Data driven simulations for accurately predicting thermodynamic properties of H2 during geological storage. Fuel **362**, 130768 (2024). DOI: https://doi.org/10.1016/j.fuel.2023.130768

[7] W. Grochala, P.P. Edwards, Thermal decomposition of the noninterstitial hydrides for the storage and production of hydrogen. Chem. Rev. **104** (3), 1283-316 (2004). DOI: https://doi.org/10.1021/cr030691s

[8] B. Sakintuna, F. Lamari-Darkrim, M. Hirscher, Metal hydride materials for solid hydrogen storage: a review. Int. J. Hydrogen Energy **32** (9), 1121e40 (2007). DOI: https://doi.org/10.1016/j.ijhydene.2006.11.022

[9] A. Pajdak, N. Skoczylas, A comparison of the kinetics of hydrogen sorption in a metallic alloy LaNi5 and in multiwall carbon nanotubes. Przemysł Chemiczny **97**, 6, 959-962 (2018). DOI: http://dx.doi.org/10.15199/62.2018.6.26

[10] R. Bardhan, A.M. Ruminski, A. Brand, J.J. Urban, Magnesium nanocrystal-polymer composites: a new platform for designer hydrogen storage materials. Energy Environ. Sci. **4** (12), 4882-95 (2011). DOI: http://dx.doi.org/10.1039/C1EE02258J

[11] L.F. Salas-Guerrero, S. Builes, G.A. Orozco, Development of atomistic graphene models for H2 adsorption from experimental data and Monte Carlo simulations. International Journal of Hydrogen Energy **50**, 1626-1633 (2024). DOI: https://doi.org/10.1016/j.ijhydene.2023.10.161

[12] A. Züttel, C. Nützenadel, P. Sudan, P. Mauron, C. Emmenegger, S. Rentsch, L. Schlapbach, A. Weidenkaff, T. Kiyobayashi, Hydrogen sorption by carbon nanotubes and other carbon nanostructures. Journal of Alloys and Compounds 330-332, 676-682 (2002). DOI: https://doi.org/10.1016/S0925-8388(01)01659-0

[13] P.A. Berseth, A.G. Harter, R. Zidan, A. Blomqvist, C.M. Araújo, R.H. Scheicher, R. Ahuja, P. Jena, Carbon Nanomaterials as Catalysts for Hydrogen Uptake and Release in NaAlH 4. Nano Letters **9** (4), 1501-1505 (2009). DOI: DOI: https://doi.org/10.1021/nl803498e

[14] G.K. Dimitrakakis, E. Tylianakis, G.E. Froudakis, Pillared Graphene: A New 3-D Network Nanostructure for Enhanced Hydrogen Storage. Nano Letters **8** (10), 3166-3170 (2008). DOI: https://doi.org/10.1021/nl801417w

[15] C. Langhammer, I. Zorić, B. Kasemo, B.M. Clemens, Hydrogen Storage in Pd Nanodisks Characterized with a Novel Nanoplasmonic Sensing Scheme. Nano Letters **7** (10), 3122-3127 (2007). DOI: https://doi.org/10.1021/nl071664a

[16] S. Park, B. Kim, Y. Lee, M. Cho, Influence of copper electroplating on high pressure hydrogen-storage behaviors of activated carbon fibers. International Journal of Hydrogen Energy **33** (6), 1706-1710 (2008). DOI: https://doi.org/10.1016/j.ijhydene.2008.01.011

[17] N.L. Rosi, J. Eckert, M. Eddaoudi, D.T. Vodak, J. Kim, M. O'Keeffe, O.M. Yaghi, Hydrogen Storage in Microporous Metal-Organic Frameworks. Science **300** (5622), 1127-1129 (2003). DOI: https://doi.org/10.1126/science.1083440

[18] G. Polak, P. Baran, J. Szczurowski, K. Zarębska, A comprehensive study on the sorption of CO2 and SO2 on modified carbon monoliths. Journal of Cleaner Production **458**, 142404 (2024). DOI: https://doi.org/10.1016/j.jclepro.2024.142404

[19] A. Pajdak, N. Skoczylas, A. Dębski, J. Grzegorek, W. Maziarz, M. Kudasik, CO2 and CH4 sorption on carbon nanomaterials and coals – Comparative characteristics. Journal of Natural Gas Science and Engineering **72**, 103003 (2019). DOI: https://doi.org/10.1016/j.jngse.2019.103003

[20] K. Hirose, M. Hirscher, Handbook of Hydrogen Storage: New Materials for Future Energy Storage, John Wiley & Sons (2010).

[21] A.G. Klechikov, G. Mercier, P. Merino, S. Blanco, C. Merino, A.V. Talyzin, Hydrogen storage in bulk graphene-related materials. Microporous and Mesoporous Materials **210**, 46-51 (2015). DOI: http://dx.doi.org/10.1016/j.micromeso.2015.02.017

[22] A. Ghosh, K.S. Subrahmanyam, K.S. Krishna, S. Datta, A. Govindaraj, S.K. Pati, C.N.R. Rao, Uptake of H2 and CO2 by graphene. J. Phys. Chem. C **112** (40), 15704-7 (2008). DOI: http://dx.doi.org/10.1021/jp805802w

[23] P. Baran, B. Buczek, K. Zarębska, Modified Activated Carbon as an Effective Hydrogen Adsorbent. Energies **15** (17), 6122 (2022). DOI: https://doi.org/10.3390/en15176122

[24] B. Panella, M. Hirscher, S. Roth, Carbon **43**, 2209-2214 (2005). DOI: http://dx.doi.org/10.1016/j.carbon.2005.03.037

[25] R.S. Rajaura, S. Srivastava, V. Sharma, P.K. Sharma, C. Lal, M. Singh, H.S. Palsania, Y.K. Vijay, Role of interlayer spacing and functional group on the hydrogen storage properties of graphene oxide and reduced graphene oxide. International Journal of Hydrogen Energy **41**, 9454-9461 (2016). DOI: https://doi.org/10.1016/j.ijhydene.2016.04.115

[26] J.W. Burress, S. Gadipelli, J. Ford, J.M. Simmons, W. Zhou, T. Yildirim, Graphene oxide framework materials: theoretical predictions and experimental results. Angew. Chem. Int. Ed. Engl. **49** (47), 8902-4 (2010). DOI: https://doi.org/10.1002/anie.201003328

[27] B.H. Kim, W.G. Hong, H.Y. Yu, Y.-K. Han, S.M. Lee, S.J. Chang, H.R. Moon, Y. Junb, H.J. Kim, Thermally modulated multilayered graphene oxide for hydrogen storage. Phys. Chem. Chem. Phys. **14** (4), 1480-4 (2012). DOI: https://doi.org/10.1039/C1CP22716E

[28] S.H. Aboutalebi, S.A. Yamini, I. Nevirkovets, K. Konstantinov, H.K. Liu, Enhanced hydrogen storage in graphene oxide-MWCNTs composite at room temperature. Adv. Energy Mater. **2** (12), 1439-46 (2012). DOI: https://doi.org/10.1002/aenm.201200154

[29] W. Liu, Y. Liu, R. Wang, Prediction of hydrogen storage on Y-decorated graphene: a density functional theory study. Appl. Surf. Sci. **296**, 204-8 (2014). DOI: https://doi.org/10.1016/j.apsusc.2014.01.087

[30] H. Zhou, J. Zhang, J. Zhang, X. Yan, X. Shen, A. Yuan, High-capacity room-temperature hydrogen storage of zeolitic imidazolate framework/graphene oxide promoted by platinum metal catalyst. Int. J. Hydrogen Energy **40** (36), 12275-85 (2015). DOI: https://doi.org/10.1016/j.ijhydene.2015.05.199

[31] M.D. Ganji, S.N. Emami, A. Khosravi, M. Abbasi, Si-decorated graphene: a promising media for molecular hydrogen storage. Appl. Surf. Sci. **332**, 105-11 (2015). DOI: https://doi.org/10.1016/j.apsusc.2015.01.151

[32] E. Durgun, S. Ciraci, T. Yildirim, Functionalization of carbonbased nanostructures with light transition-metal atoms for hydrogen storage. Phys. Rev. B **77** (8), 085405-14 (2008). DOI: https://doi.org/10.1103/PhysRevB.77.085405

[33] T. Mashoff, M. Takamura, S. Tanabe, H. Hibino, F. Beltram, S. Heun, Hydrogen storage with titanium-functionalized graphene. Appl. Phys. Lett. **103** (1), 013903-4 (2013). DOI: https://doi.org/10.1063/1.4812830

[34] A. Liu, S. Liu, Hydrogen sorption and diffusion in coals: Implications for hydrogen geo-storage. Applied Energy (2023). DOI: https://doi.org/10.1016/j.apenergy.2023.120746

[35] M. Sayyafzadeh, M. Camilleri, D. Heryanto, R. Sander, Coal Seams as an In-Situ Filter for Hydrogen Separation. APOGCE (2024). DOI: https://doi.org/10.2118/221195-ms

[36] K. Czerw, P. Baran, J. Szczurowski, K. Zarębska, Sorption and Desorption of CO2 and CH4 in Vitrinite- and Inertinite-Rich Polish Low-Rank Coal. Natural Resources Research **30**, 543-556 (2021). DOI: https://doi.org/10.1007/s11053-020-09715-2

[37] N. Skoczylas, A. Pajdak, M. Kudasik, L. Braga, CH4 and CO2 sorption and diffusion carried out in various temperatures on hard coal samples of various degrees of coalification. Journal of Natural Gas Science and Engineering **81**, 103449 (2020). DOI: https://doi.org/10.1016/j.jngse.2020.103449

[38] A. Dudzińska, Sorption properties of hard coals with regard to gases present in the mine atmosphere. Journal of Earth Science **28**, 124-130 (2017). DOI: https://doi.org/10.1007/s12583-016-0716-2

[39] K. Kozieł, N. Skoczylas, Experimental analysis of rock mass transport during dolomite and gas outburst. International Journal of Rock Mechanics and Mining Sciences **185**, 105969 (2025). DOI: https://doi.org/10.1016/j.ijrmms.2024.105969

[40] N. Skoczylas, M. Kudasik, A. Pajdak, L. Teixeira Palla Braga, Study of CO2/CH4 exchange sorption in coal under confining pressure conditions. International Journal of Greenhouse Gas Control **124**, 103845 (2023). DOI: https://doi.org/10.1016/j.ijggc.2023.103845

[41] M. Wierzbicki, A. Pajdak, P. Baran, K. Zarębska, Isosteric heat of sorption of methane on selected hard coals. Przemysł Chemiczny **98**, 4 625-629 (2019). DOI: http://dx.doi.org/10.15199/62.2019.4.22

[42] S. Chattaraj, D. Mohanty, T. Kumar, G. Halder, Thermodynamics, kinetics and modeling of sorption behavior of coalbed methane – A review. Journal of Unconventional Oil and Gas Resources **16**, 16-33 (2016). DOI: https://doi.org/10.1016/j.juogr.2016.09.001

[43] J. Liu, C. Wang, X. He, S. Li, Infrared measurement of temperature field in coal gas desorption. Int. J. Min. Sci. Technol. **24**, 57 (2014). DOI: https://doi.org/10.1016/j.ijmst.2013.12.010

[44] G. Yue, Z. Wang, X. Tang, H. Li, C. Xie, Physical Simulation of Temperature Influence on Methane Sorption and Kinetics in Coal (II): Temperature Evolvement during Methane Adsorption in Coal Measurement and Modeling. Energy Fuels **29**, 6355 (2015). DOI: https://doi.org/10.1021/acs.energyfuels.5b01637

[45] H. Li, J. Kang, F. Zhou, Z. Qiang, G. Li, Adsorption heat features of coalbed methane based on microcalorimeter. J. Loss Prev. Process Ind. **55**, 437-449 (2018). DOI: https://doi.org/10.1016/j.jlp.2018.05.006

[46] J. Deng, J. Kang, F. Zhou, H. Li, D. Zhang, G. Li, The adsorption heat of methane on coal: Comparison of theoretical and calorimetric heat and model of heat flow by microcalorimeter. Fuel **237**, 81 (2019). DOI: https://doi.org/10.1016/j.fuel.2018.09.123

[47] T. Horikawa, Y. Zeng, D.D. Do, K. Sotowa, J.R.A. Avila, On the isosteric heat of adsorption of non-polar and polar fluids on highly graphitized carbon black. Journal of Colloid and Interface Science **439**, 1 (2015). DOI: https://doi.org/10.1016/j.jcis.2014.10.024

[48] S.H. Madani, S. Sedghi, M.J. Biggs, P. Pendleton, Analysis of Adsorbate-Adsorbate and Adsorbate-Adsorbent Interactions to Decode Isosteric Heats of Gas Adsorption. ChemPhysChem **16**, 3797 (2015). DOI: https://doi.org/10.1002/cphc.201500881

[49] A. Gajda, P. Jodłowski, K. Kozieł, G. Kurowski, K. Hyjek, N. Skoczylas, A. Pajdak, Adsorption of selected GHG on metal-organic frameworks in the context of accompanying thermal effects. Archives of Environmental Protection **50**, 4, 51-63 (2024). DOI: https://doi.org/10.24425/aep.2024.152895

[50] C. Guan, S. Liu, C. Li, Y. Wang, Y. Zhao, The temperature effect on the methane and CO2 adsorption capacities of Illinois coal. Fuel **211**, 241-250 (2018). DOI: https://doi.org/10.1016/j.fuel.2017.09.046

[51] A. Gajda, A. Pajdak, N. Skoczylas, M. Kudasik, K. Kozieł, G. Kurowski, K. Hyjek, K. Dymek, M. Sitarz, P. Jodłowski, Effective heat transfer associated with CO2 and CH4 adsorption on HKUST-1 metal-organic framework deposited in situ on heat exchanger. Energy **307**, 132525 (2024). DOI: https://doi.org/10.1016/j.energy.2024.132525

[52] C.M. White, D.H. Smith, K.L. Jones, A.L. Goodman, S.A. Jikich, R.B. LaCount, S.B. DuBose, E. Ozdemir, B.I. Morsi, K.T. Schroeder. Sequestration of carbon dioxide in coal with enhanced coalbed methane recovery – A review. Energy & Fuels **19** (3), 659-724 (2005). DOI: https://doi.org/10.1021/ef040047w

[53] A.L. Myers, Thermodynamics of Adsorption in Porous Materials. AIChE Journal **48**, 1, 145-160 (2002). DOI: http://dx.doi.org/10.1002/aic.690480115

[54] Y.W. Zhu, S. Murali, M.D. Stoller, K.J. Ganesh, W.W. Cai, P.J. Ferreira, A. Pirkle, R.M. Wallace, K.A. Cychosz, M. Thommes, D. Su, E.A. Stach, R.S. Ruoff, Carbon-based supercapacitors produced by activation of graphene. Science **332** (6037), 1537-1541 (2011). DOI: http://dx.doi.org/10.1126/science.1200770

[55] UN-ECE International Classification of In-Seam Coals, UNECE Geneva. UN New York 1998:41.

[56] K. Kozieł, A. Gajda, M. Skiba, N. Skoczylas, A. Pajdak, Influence of grain size and gas pressure on diffusion kinetics and CH4 sorption isotherm on coal. Archives of Mining Sciences **69**, 1, 3-23 (2024). DOI: https://doi.org/10.24425/ams.2024.149824

[57] M. Gawor, N. Skoczylas, A. Pajdak, M. Kudasik, Nonlinear and Linear Equation of Gas Diffusion in Coal – Theory and Applications. Applied Sciences **11**, 5130 (2021). DOI: https://doi.org/10.3390/app11115130

[58] M. Kudasik, The manometric sorptomat – an innovative volumetric instrument for sorption measurements performed under isobaric conditions. Measurement Science and Technology **27**, 3, 035903 (2016). DOI: https://doi.org/10.1088/0957-0233/27/3/035903